Cranked self-consistent mean-field description of the triaxially deformed rotational bands in ^{138}Nd

Yue Shi (石跃)*
Department of Physics, Harbin Institute of Technology, Harbin 150001, People's Republic of China

(Received 26 September 2018; revised manuscript received 25 November 2018; published 4 March 2019)

Background: Compared to the axially deformed nuclei, triaxially deformed ones are relatively scarce. This is mainly due to the difficulties in the identification of experimental signatures pertaining to the triaxial degree of freedom. In the nucleus ^{138}Nd, a number of rotational bands have been observed to have medium or high spin values. They have been interpreted in the macroscopic-microscopic method, to be based on triaxial minima. In particular, for a few configurations, the calculations suggested that a reorientation of the rotational axis may have occurred along the rotational bands.
Purpose: The present work aims at a quantitative description of the experimentally observed bands in ^{138}Nd, using the cranked self-consistent Skyrme-Hartree-Fock (SHF) method or cranked nuclear density functional theory (DFT). Such a study, which is still missing, will provide alternative interpretations of the structure of the bands and hence, shed new light on the triaxiality issue in connection with experimental data.
Methods: The rotational bands are described using cranked self-consistent mean-field method with SLy4 and SkM* Skyrme energy density functionals (EDFs). For SLy4 EDF, the time-odd pieces are included using Landau parameters (denoted with SLy4$_{\rm L}$). For SkM* EDF, the local gauge invariance argument has been used to determine the time-odd components of the mean field.
Results: The survey of different configurations near Fermi surface of ^{138}Nd results in 12 lowest configurations, at both positive- and negative-γ deformations. These are calculated to be the energetically lowest configurations. The results show that, for both EDFs, the rotational states based on positive-γ minimum, which is at $\gamma \approx 35^\circ$, are lower than the respective configurations with negative-γ deformation. The general trends of the spin-versus-ω curve, and the energy-versus-spin curve reproduce well those of the experimental data. Further, for the observed bands T1–T8, the calculated results using SLy4$_{\rm L}$ allows the configurations of the observed bands to be assigned. The calculations predict transitional quadrupole moments, which can be used to compare with future experimental data.
Conclusions: The current cranked self-consistent mean-field calculations of the near-yrast high-spin rotational bands in ^{138}Nd reproduce well the experimental data. The results suggest that the experimentally observed bands can be assigned to the calculated bands with various configurations at the positive-γ deformation. The predictions of the current calculations are complementary to that of the well-known macroscopic-microscopic calculations, both of which await future experiment to verify.

DOI: 10.1103/PhysRevC.99.034304

I. INTRODUCTION

It has been known that the occurrence of rotational bands in a nucleus is due to the break of rotational invariance of the nuclear mean-field Hamiltonian in the intrinsic frame [1,2]. There are a few fascinating phenomena that can be associated with the triaxial deformation of a nucleus. Among them, the energy inversion of the signature partners, differing from a normal order predicted by rotational models without the triaxial deformation [3]; the occurrence of identical bands, which are presumably due to the break of chiral symmetry in a triaxially deformed mean field [4,5]; as well as the bands based on wobbling motions of a rotating nucleus [6] are perhaps the most significant examples.

Compared to the axially symmetric deformation, where the characterization has been fairly well established both experimentally and theoretically, physics associated with triaxially deformed nuclei has been rather scarce. This is due to the more subtle experimental signatures associated with the triaxial degree of freedom. Indeed, alternative explanations may coexist to explain those phenomena postulated to be due to triaxial deformation. In particular, for states near ground states, a triaxially deformed nucleus tend to have soft minima in the potential-energy surface, where ambiguities arises as to weather the observed triaxial deformations are of a static character.

Recently, in the Er-158 nuclear region, a number of strongly triaxially deformed bands (TSD) have been observed to have large dynamic moments of inertia, marking the return of collectivity in these nuclei, in which core-breaking excitations were observed [7–11]. In the macroscopic-microscopic calculations [12], these bands were calculated to be associated with triaxially deformed minima. In the two triaxially deformed minima, the tilted-axis-cranked self-consistent mean-field calculations [13,14] suggested that the energetically

*yueshi@hit.edu.cn

higher minimum is unstable with respect to a reorientation of the rotational axis. However, these strongly triaxial deformed bands were not linked to the lower-energy states where spin and energy values are known, leaving the spin and energy values of these TSD bands underdetermined. This makes the interpretations of the theoretical models uncertain [15].

A much better laboratory for studying the triaxially deformed nucleus may be ^{138}Nd. Indeed, in this nucleus, a multitude of rotational bands have been observed [16–19]. For them, the macroscopic-microscopic model [12] has predicted a rather pronounced static triaxial deformation. In particular, the linking transitions from these band members to the energetically known lower-spin states have been observed through precise γ-ray measurements. Consequently, the spin values and the excitation energies of the bands have been determined, which provide much better testing ground for theoretical models compared to the situation of ^{158}Er.

Incidentally, the macroscopic-microscopic calculations in Ref. [18] showed that the structural changes in a pair of the rotational bands in ^{138}Nd were due to the deformation change from a positive-γ value to a negative-γ one. These findings may constitute the first observation of the reorientation effect of the rotational axis with increasing rotational frequency. It is then desirable to see the predictions from alternative theoretical models, such as the self-consistent mean-field methods [15,20], which is still missing.

The present work aims at a description of the observed bands in Refs. [17,19] using a cranked nuclear density functional theory (DFT). The alternative description of the observables is supposed to shed new light on the underlying structures of these bands, leading to a better understanding of triaxial deformation in nuclear structure. In Sec. II, I describe the model, and the parameter used in the current work. Section III presents detailed results and discussions, before a summary, which is presented in Sec. IV.

II. MODEL

In the present work, the cranked SHF calculations are performed with symmetry-unrestricted solver HFODD (version 2.49t [21]). In this model, the total energies (or Routhians in the rotational frame [22]) are represented as functional of various densities [20]. The single-particle Hamiltonian is expanded in terms of 969 deformed harmonics oscillator basis, which are $\hbar\omega_x = \hbar\omega_y = 0.4945$, and $\hbar\omega_z = 0.4499$ MeV.

The SkM* [23] and SLy4 [24] energy density functionals (EDFs) are used in the particle-hole channel of the cranked SHF problem. For cranking calculations, one deals with nonzero time-odd densities and fields. The coupling constants are determined using local gauge invariance arguments [25], and Landau parameters [26], for SkM* and SLy4 EDFs, respectively. The latter is then denoted with SLy4$_{\rm L}$. The current choice of the parametrizations including the time-odd part is identical with those appeared in Refs. [13,14] for consistency.

To obtain the solutions corresponding to the local minima that are interesting for the current work, calculations with constraints on the quadrupole moments, Q_{20} and Q_{22}, are first performed. The constraints on Q_{20} and Q_{22} deformations are then removed by zeroing the respective Lagrangian multipliers. The earlier constraint solutions are used to warm start the deformation unconstrained calculations.

TABLE I. The SHF configurations in ^{138}Nd studied in this work. Each configuration is described by the number of states occupied in the four parity-signature (π, ρ) blocks, in the convention defined in Ref. [27]. For configurations 07 and 08, the $18 \rightarrow 19$ means that the neutron is moved from the 18th to the 19th level. The transition quadrupole moment, Q_t values, are calculated using the SLy4$_{\rm L}$ EDF at $\hbar\omega = 0.6$ MeV for the positive-γ deformed minimum. The Q_t values are calculated through the relation $Q_t = Q_{20}^p + \sqrt{\frac{1}{3}}Q_{22}^p$.

Label	Configuration	π	ρ	Q_t (eb)
01	$\nu[20, 20, 19, 19] \otimes \pi[16, 16, 14, 14]$	+	+1	2.7
02	$\nu[19, 21, 19, 19] \otimes \pi[16, 16, 14, 14]$	+	−1	3.2
03	$\nu[20, 20, 19, 19] \otimes \pi[16, 15, 15, 14]$	−	−1	3.0
04	$\nu[20, 21, 19, 18] \otimes \pi[16, 15, 15, 14]$	+	−1	3.5
05	$\nu[21, 20, 18, 19] \otimes \pi[16, 16, 14, 14]$	−	+1	2.6
06	$\nu[21, 20, 19, 18] \otimes \pi[16, 16, 14, 14]$	−	−1	2.6
07	$\nu[21, 20, 18 \rightarrow 19, 19] \otimes \pi[16, 16, 14, 14]$	−	+1	2.2
08	$\nu[21, 20, 19, 18 \rightarrow 19] \otimes \pi[16, 16, 14, 14]$	−	−1	2.3
09	$\nu[20, 20, 19, 19] \otimes \pi[15, 16, 14, 15]$	−	−1	2.7
10	$\nu[20, 21, 19, 18] \otimes \pi[16, 16, 14, 14]$	−	+1	3.0
11	$\nu[20, 21, 18, 19] \otimes \pi[16, 16, 14, 14]$	−	−1	3.0
12	$\nu[20, 20, 19, 19] \otimes \pi[16, 15, 14, 15]$	−	+1	3.0

In the current principal-axis-cranking calculations, parity and signature symmetries are always enforced. Each single-particle level could be labeled by parity and signature quantum numbers. For details, see the caption of Table I.

Before I end this section, some explanations about (i) the sign of the γ value, which is used to measure the degree of triaxial deformation, and (ii) the relation between the commonly accepted convention (Lund convention) and the one used in the current work is necessary. In the Lund convention, the rotation is chosen to be around the x axis and the deformation with γ value in the interval of $(0, 60^\circ)$ corresponds to a triaxially deformed nucleus that rotates around its short axis [2].

In the HFODD code [22], the one-dimensional cranking is around the y axis, and the Q_{22} value is defined as $\sqrt{3}\langle\hat{x}^2 - \hat{y}^2\rangle$. In the current calculation, the minima with positive-Q_{22} values are identified as minima with positive-γ values. This definition is consistent with the Lund convention in the fact that, for both conventions, a positive-γ value indicates rotation around its short axis.

To fully conform with the Lund convention, which uses x axis as the cranking axis, a final step one needs to do is the following relabeling of the axes in the HFODD code: $(x, y, z) \rightarrow (y, x, -z)$. This results in the change of the sign of Q_{22} value. Such a convention transformation in the present calculations has been carefully considered. Note the negative sign in front of Q_{22} in Fig. 3 of Ref. [13], and in the current work.

III. RESULTS AND DISCUSSIONS

Table I lists the configurations in ^{138}Nd studied in this work. Note that for each configuration, there are two states corresponding to the minima with positive- and negative-γ

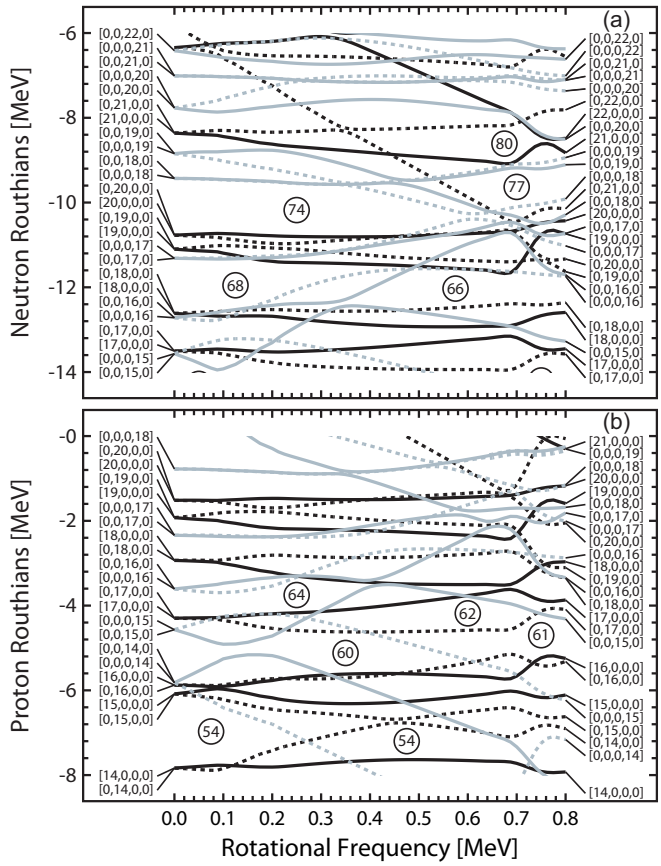

FIG. 1. Single-particle Routhians from cranked SHF calculations with $SLy4_L$ EDF for $^{138}_{60}Nd_{78}$. The configuration is pg01 in Table I. The quadrupole moments for rotational frequencies between 0.4–0.8 MeV are $(Q_{20}, Q_{22}) \approx (10.0, 5.3)$ b. The levels with positive and negative parities are indicated by black and light gray lines, respectively. The levels with $+i$ and $-i$ signatures are indicated by solid and dashed lines, respectively. One could find the order of the level within its (π, ρ) block at the beginning and the end of each line.

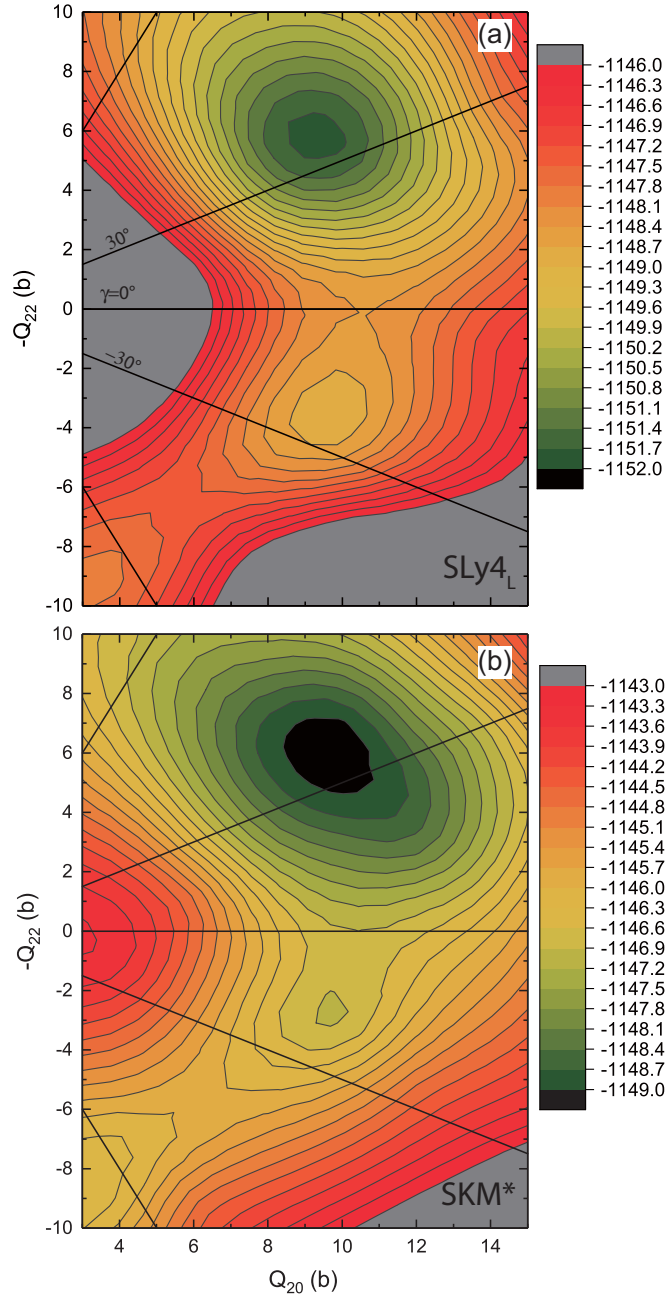

FIG. 2. Total Routhian surfaces for ^{138}Nd for configuration pg01 in Table I. Calculations are performed with (a) Skyrme EDF $SLy4_L$, and (b) SkM* at a rotational frequency of 0.6 MeV. Contour lines are 0.4 MeV apart in energy.

values. In the following discussions, the 01 configuration with a positive-γ minimum is denoted with pg01, the negative-γ one is denoted with ng01. The same rule of naming is applied to other configurations.

In Fig. 1, I show the calculated single-particle Routhians for $SLy4_L$ calculated with configuration pg01 listed in Table I. It can be seen that the configuration pg01 contains no particle-hole excitations for the frequency interval of ∼0.0–0.5 MeV. It has to be noted that, even though the configuration pg01 appears to be the lowest energetically, since the single-particle levels below the Fermi surfaces of protons and neutrons are occupied, it does not necessarily indicate that the obtained total energy of this configuration in the rotating frame is the lowest. This is so because a state with another configuration may acquire additional binding through self-consistent process. In addition, a state with another configuration may be lower in energy by having a slightly different deformation compared to the configuration pg01.

Nevertheless, it is reasonable to state that configuration pg01 is among the lowest in total Routhian for frequency interval of ∼0.0–0.5 MeV, which will be shown in the energy-versus-spin plot in later discussions. In Fig. 1, it can be seen that, for $\hbar\omega > 0.5$ MeV, a state with $(\pi, \rho) = (+, -i)$ penetrates below the neutron Fermi surface, and crosses with the 20th level in the $(+,-i)$ block at $\hbar\omega \sim 0.7$ MeV. This crossing corresponds to the characteristic back-bending observed in the experimental data, which will be discussed later. The behaviors of spin and energy values as a function of rotational frequency of configuration pg01 are rather typical. Hence, the quality of the description of these behaviors are particularly

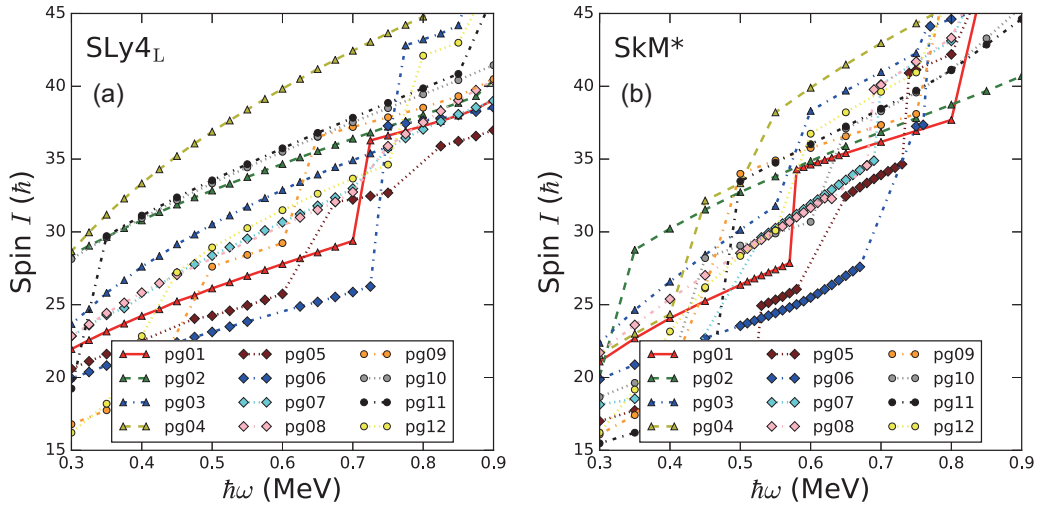

FIG. 3. The total angular momenta as a function of rotational frequency for different configurations at positive-γ values as a function of rotational frequency calculated with SLy4$_L$ and SkM* EDFs. The solid, dashed, dotted, and dotted-dashed lines denote states with $(\pi, \rho) = (+, 0), (+, +1), (-, 0)$, and $(-, +1)$, respectively.

important for assessing the usefulness of the current calculations.

Before showing the calculated total angular momenta and energies as a function of rotational frequency, in Fig. 2, I show the total-Routhian surfaces of ^{138}Nd for configuration 01 in Table I, calculated with SLy4$_L$ [24] [Fig. 2(a)], and SkM* [23] [Fig. 2(b)] EDFs, at a rotational frequency of 0.6 MeV. For both EDFs, the minima at the positive- and negative-γ deformations can be seen. The minima with positive-γ values are deeper, and are larger in terms of $|\gamma|$ value. For SLy4$_L$, the positive-γ minimum is deeper than that of the negative-γ one by $\sim$3.0 MeV in energy. Whereas the energy difference for the two minima of SkM* is only $\sim$1.5 MeV. The barrier separating the two minima in the γ direction is lower for SkM* compared to that of SLy4$_L$. Note that for SkM* EDF, the crossing with the lowest level from $\mathcal{N} = 6$ states has already happened (see below for the crossing rotational frequency). For SLy4$_L$ EDF, this crossing happens at a larger rotational frequency ($\hbar\omega \approx 0.7$ MeV) for this configuration.

Figure 3 shows the total spin values for the configurations listed in Table I, that are at the positive-γ deformation (see Fig. 2), as a function of rotational frequency. It can be seen that the angular momenta are in the range of 20–45 $\hbar$ for $\hbar\omega >$ 0.5 MeV. For several configurations, a characteristic sudden increase of angular momenta can be seen. This is due to the repel between the $\mathcal{N} = 6$ level, and the level below it in the same (π, ρ) block at $\hbar\omega \approx 0.7$ MeV, as shown in Fig. 1. For SkM* EDF [Fig. 3(b)], the alignment for the configuration 01 occurs at a smaller rotational frequency, $\hbar\omega \approx 0.6$ MeV.

In Fig. 4, the same quantities as those in Fig. 3 are plotted, except that these states have negative-γ values. Compared to the same configurations at positive-γ deformation, the spin values for all configurations, and for both EDFs, increase faster with increasing $\hbar\omega$. In addition, the sudden increase of

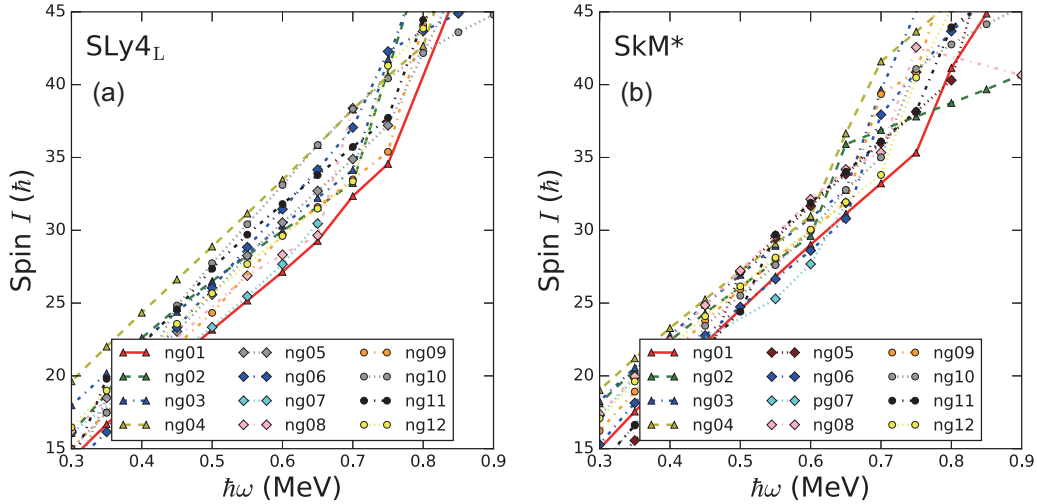

FIG. 4. The total angular momenta for different configurations at negative γ values as a function of rotational frequency calculated with SLy4$_L$ and SkM* EDFs.

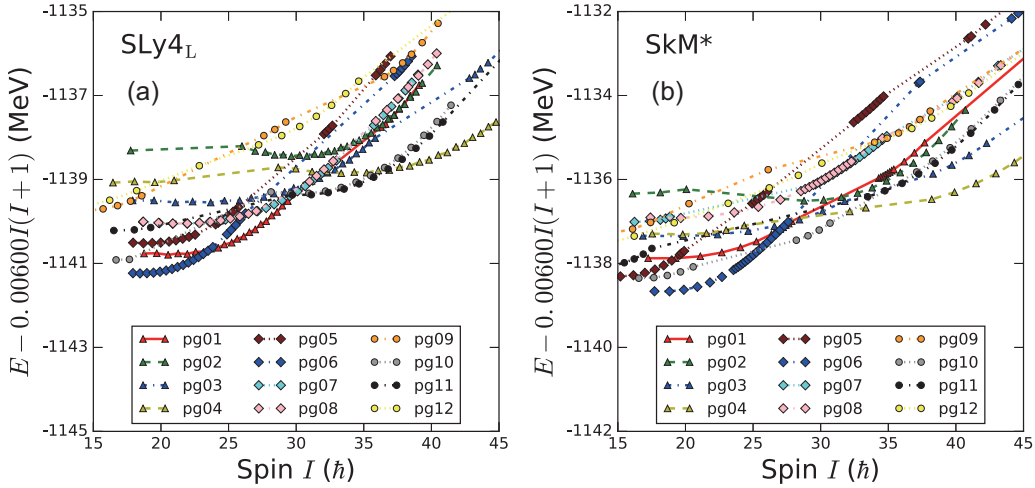

FIG. 5. Total energies for different configurations at positive γ values. Results are calculated with SLy4$_L$ and SkM* EDFs.

spin at certain ω values is less abrupt (or absent), as shown in Fig. 3.

It has to be noted that, in this mean-field study, the total spin values are determined by summing the individual contributions from occupied single-particle levels. Hence, the total spin values are rather sensitive to the calculated deformation and the specific configurations. This can be seen by comparing Figs. 3 and 4, which correspond to angular momenta variations as functions of rotational frequency at two different deformations. It can be seen that the total spin values for the same EDF, at the same frequency values, and for the same configuration can differ up to $\sim 10\hbar$. The variation as functions of rotational frequency is also different for the same EDF, and the same configuration.

Figure 5 displays the total energies of ^{138}Nd for configurations listed in Table I at the positive-γ deformation, calculated with SLy4$_L$ [Fig. 5(a)], and SkM* [Fig. 5(b)] EDFs. For each configuration, the energy of an arbitrary rotor has been subtracted from the total energy. This is to bring the curves less steep for viewing the detail of the curves more clearly. It can be seen that both EDFs predict similar trends for same configurations. In addition, the alignments that have been seen in the spin-versus-frequency figure (Fig. 3) are reflected in these energy-versus-spin curves, as a subtle change of the slopes. This can be understood as the sudden increase of the moments of inertia, which results in the decrease of energies that are needed to provide the same amount of spin increase.

Figure 6 shows the same quantities as those in Fig. 5, except for negative-γ values. It can be seen that the changes due to the abrupt spin changes are absent in these bands. Comparing the energies of the same configuration, it can be seen that the energies on the negative-γ side are in general 1–2 MeV higher than that of their positive-γ states. For SkM* EDF, the ng02 shows a large change. This is because the self-consistent calculation follows the positive-γ minimum.

Figure 7 compares the experimental spin values [Fig. 7(a)] of the rotational bands, extracted from Ref. [19], with the present cranked DFT calculations using SLy4$_L$ EDF [Fig. 7(b)]. The calculated spin values are extracted from Figs. 3(a) and 4(a). It can be seen that the calculations display

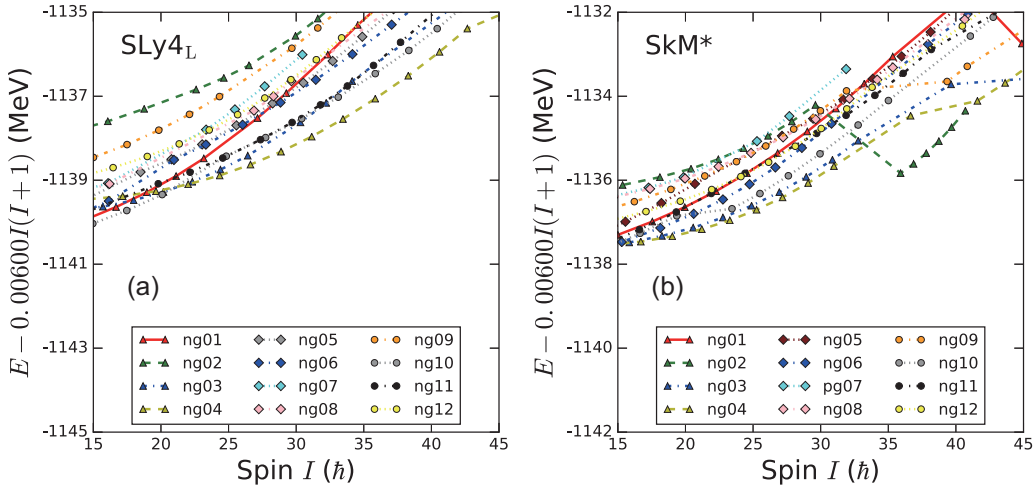

FIG. 6. Same as Fig. 5, except that the curves correspond to the configurations with negative γ values.

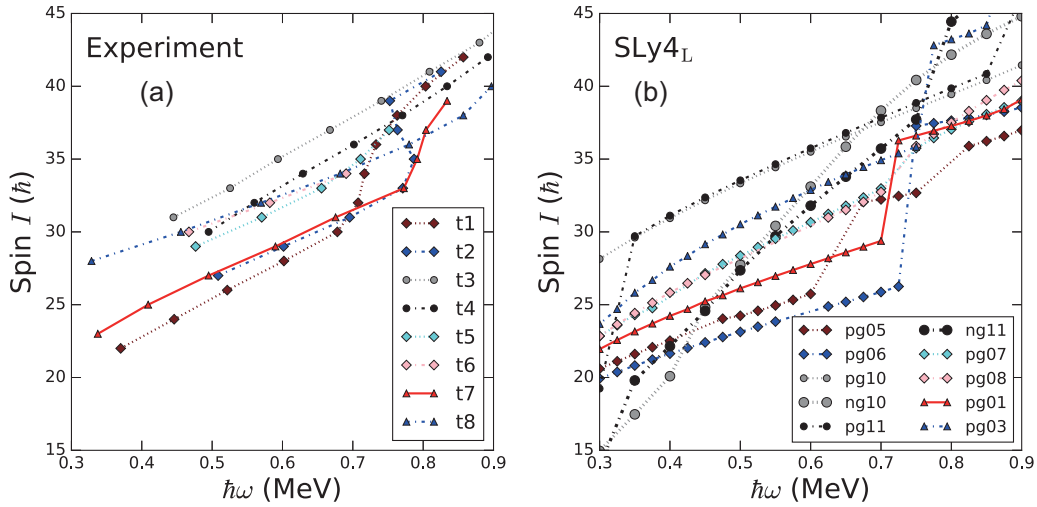

FIG. 7. Experimental angular momenta as a function of rotational frequency (a) for t1-t8 bands from Ref. [19]. The $\hbar\omega$ values for $E(I)$ values are evaluated as $\frac{1}{2}E_\gamma(I+1\rightarrow I-1)$. The calculated values (b) are extracted from Figs. 3(a) and 4(a). The proposed configuration assignment of the current work for the experimental data are indicated by labeling the respective calculated curve with the same type of markers. See text for the case of t3 and t4 bands.

general consistencies with data in terms of both the trend and the absolute values. In particular, both data and the calculations show characteristic up-bends at certain rotational frequency. Specifically, the spin values of T7 band up-bend at $\hbar\omega \approx 0.75$ MeV. The calculations underestimate this rotational frequency by about 0.15 and 0.25 MeV for SLy4$_L$ [Fig. 3(a)] and SkM* [Fig. 3(b)] EDFs, respectively.

Note that this alignment in the present calculation is mainly due to the crossing of the $\mathcal{N}=6$ state with the lower state in the same (π,ρ) block. It is rather sensitive to the parameter used, and in particular, the predicted deformations of the minima. Hence, the critical frequency at which the alignment occurs could be used as a criterion for assessing the usefulness of a given parameter set used. One may use this quantity to adjust parametrization if one needs to constrain on the single-particle properties.

The transitions linking the high-spin states to states with lower spins have been observed in Refs. [19]. This allows for the excitation energies and the spin values to be determined. To compare these data with the calculations, one needs to calculate the ground state of ^{138}Nd where pairing interaction is present. In Table II, I list the calculated ground-state total energies, and the pairing properties for ^{138}Nd with SLy4$_L$ and SkM* EDFs. The calculation setup is identical to those used to calculate the rotational bands, except that for the calculations of the ground states, the pairing correlations are included through the Skyrme-Hartree-Fock-Bogoliubov method [28]. The pairing cutoff energies are $E_{\rm cutoff}=60$ MeV, for both protons and neutrons. The pairing strengths are determined to reproduce the experimental odd-even staggering energies, which are 1.07, and 1.15 MeV for neutrons, and protons, respectively.

TABLE II. The calculated total energies, pairing gaps, Fermi energies, and quadrupole moments for the ground state of ^{138}Nd using SHFB method.

	SLy4$_L$	SkM*
$E_{\rm tot}$ (MeV)	−1145.207	−1141.870
Δ_n (MeV)	1.03	1.06
Δ_p (MeV)	1.06	1.10
λ_n (MeV)	−9.806	−9.696
λ_p (MeV)	−4.520	−4.018
Q_{20} (e b)	2.62	2.90
Q_{22} (e b)	0.00	1.15

In Fig. 8, I compare the observed excited energies [19] [Fig. 8(a)] with the calculated ones with SLy4$_L$ EDF, the latter of which are extracted from Figs. 5(a) and 6(b). It can be seen from Fig. 8 that the present calculations [Fig. 8(b)] systematically underestimate the observed excited energies of the bands [Fig. 8(a)] by ∼1.5 MeV for SLy4$_L$ EDF. It should be noted that the calculations with SLy4$_L$ EDF predict prolate ground state, whereas the results using SkM* EDF suggest a well-deformed triaxial deformation for the ground state. One needs to note that the current description may be insufficient for this nucleus near ground state, which has soft potential-energy surface. Additional effects such as the vibrational motions may invite further correlations on the current mean-field results.

Compared to the absolute energies, better indicators of a successful description of rotational bands are (i) the relative energies between the bands, and (ii) the trend of the total energies as a function of spin values. Taking into account of these two criteria (see Fig. 8), together with the spin-versus-ω plots (see Fig. 3) allow one to assign the experimentally observed bands [19] T1, T2, T3, T4, T5, T6, T7, and T8 to the calculated ones with configurations pg05, pg06, pg10/ng10, pg11/ng11, pg07, pg08, pg01, and pg03, respectively. For positive configurations other than those included in Table I, the calculations predict rather high particle-hole configurations. This is due to the opposite parity states of both protons

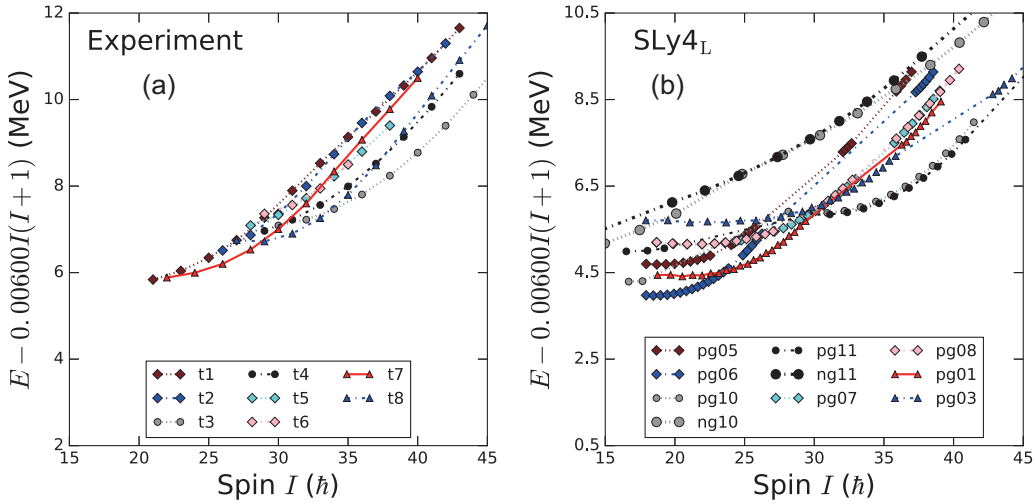

FIG. 8. Total energies as a function of angular momenta extracted from experimental data [16,19,29], compared with the SLy4$_L$ shown in Fig. 5. The energy values are plotted with respect to the energy of the 22^+ state of T7. The calculated values (b) are extracted from Figs. 5(a) and 6(a).

and neutrons for the single-Routhian states, above and below the Fermi surfaces, as shown in Fig. 1. To create a positive one-particle-one-hole state, a neutron or proton needs to be excited across the opposite states above the Fermi surface, which results in high excitation energies.

There are a few interesting points worth mentioning along with the assignments. First, the present calculations predict a yrast band with pg01 configuration for the spin values in the interval of ∼24–30$\hbar$. For spin values lower than 24$\hbar$, configuration pg06 is lower in energy. For higher spin values ($I \geqslant 30\hbar$), the yrast status of pg01 is taken over by signature partners pg10,11. This is consistent with the data, as shown in Fig. 8. For the near yrast states, the good agreement between the calculations and the data [19] for spin values larger than 20$\hbar$ is important for evaluating the predictions of the current calculations. For spin values between 20$\hbar$ and 25$\hbar$, the experimental information on band t2 is still missing, which prevents a direct comparison between experimental data (t2) and the calculations (pg06), see Fig. 8.

Second, a close examination of the experimental curve T7 and the curve with pg01 configuration, reveals a change of the slope in the spin range of 30–35$\hbar$. This is, in the current calculation, interpreted to be due to the alignment of neutrons at $\hbar\omega \approx 0.7$ MeV (see Fig. 3). The interpretation is similar for T1, and T2 bands, where the calculations predict that the variations in the energy curves are due to alignment. This differs from the interpretation in Ref. [18], where the macroscopic-microscopic calculations suggested a transition of the minimum from a positive- to a negative-γ deformation.

Third, if one assigns T3, and T4 to pg10, and pg11, respectively, then one finds that the energy curves show slower increase with increasing spin values compared to the experiment, as shown in Fig. 8. The calculated angular momenta seem to have a smaller slope compared to data, see Fig. 7. However, the energy curves and the spin curves corresponding to the negative-γ deformation seem to overestimate the slopes of the curves of experimental data.

To verify the second and third interpretations raised by the current calculations, one needs to conduct experimental measurements of the transitional quadrupole moments or life time on the bands T1, 2, 3, 4, 7, as well as a few other states for references. Table III lists the transitional quadrupole moments

TABLE III. Calculated proton quadrupole moments in ^{138}Nd for different configurations, with SLy4$_L$ EDF. The pg, and ng denote positive-, and negative-γ minima, respectively.

Band	$\hbar\omega$	Q^p_{20} (eb)		$-Q^p_{22}$ (eb)		Q_t (eb)		J ($\hbar$)	
	(MeV)	pg	ng	pg	ng	pg	ng	pg	ng
01	0.4	4.3	4.8	2.2	−1.6	3.0	5.7	24.2	19.0
	0.5	4.2	4.7	2.3	−1.5	2.9	5.6	26.1	23.2
	0.6	4.0	4.6	2.3	−1.4	2.7	5.4	27.8	27.1
	0.7	3.9	4.3	2.4	−1.2	2.5	5.0	29.4	32.3
	0.8	4.0	4.5	2.9	−1.2	2.3	5.2	37.3	44.3
05	0.4	3.8	4.6	2.0	−1.3	2.6	5.4	22.5	20.8
	0.5	3.6	4.5	2.1	−1.1	2.4	5.1	24.2	25.6
	0.6	3.5	4.2	2.2	−0.9	2.2	4.7	25.7	30.5
	0.7	3.4	4.0	2.3	−0.8	2.1	4.6	32.2	34.9
06	0.4	3.7	4.6	2.0	−1.3	2.5	5.4	21.6	21.0
	0.5	3.6	4.4	2.1	−1.1	2.4	5.0	23.1	26.0
	0.6	3.5	4.1	2.1	−1.0	2.3	4.7	25.1	31.5
	0.7	3.3	3.7	2.1	−1.0	2.1	4.3	25.9	37.1
	0.8	3.3	2.5	1.8	−1.4	2.3	3.3	37.6	43.7
10	0.4	4.7	4.1	2.2	−1.4	3.4	4.9	30.9	20.1
	0.5	4.5	4.3	2.3	−1.1	3.2	4.9	33.3	27.7
	0.6	4.4	4.0	2.4	−1.0	3.0	4.6	35.5	33.1
	0.7	4.2	3.6	2.4	−1.1	2.8	4.2	37.5	38.3
	0.8	4.1	3.2	2.5	−1.1	2.7	3.8	39.5	42.2
11	0.4	4.7	4.6	2.2	−1.3	3.4	5.4	31.1	22.2
	0.5	4.5	4.4	2.3	−1.1	3.2	5.0	33.5	27.4
	0.6	4.4	4.1	2.4	−1.0	3.0	4.7	35.7	31.8
	0.7	4.2	3.9	2.4	−0.9	2.8	4.4	37.8	35.7
	0.8	4.0	3.6	2.5	−1.0	2.6	4.2	39.9	44.4

calculated with $SLy4_L$ at both positive- and negative-γ values for a few configurations. Incidentally, a recent experiment [30] performed interesting life-time measurement on the rotational bands near ground state of ^{138}Nd. The current work suggests that the lifetime data in the spin intervals of 30–40$\hbar$ are highly desirable. A comparative study among the bands with spin increase, together with theoretical calculations will reveal better modelings, better parameterizations, as well as suitable testing grounds for phenomena such as shape transitions, rotational axis re-orientations, alignments with triaxial shape, all in the same nucleus.

IV. SUMMARY

In the current work, cranked self-consistent Skyrme-Hartree-Fock (SHF) calculations were applied to the description of the rotational bands recently observed in ^{138}Nd in the spin range of 20–45$\hbar$. For the configurations near yrast line, the calculations with both SkM* and $SLy4_L$ parameters predicted pronounced triaxial minima at positive-γ deformation and comparatively soft triaxial minima at negative-γ deformation. The configurations with positive-γ deformation were calculated to be lower in energy compared to those with negative-γ deformation for both parameters.

By comparing the calculated total angular momenta as a function of rotational frequency and the relative total energies as a function of spin values for different configurations with experimental data, the configurations of the observed bands [19] T1–8 were assigned in the current cranked SHF calculations. It needs to be noted that for some configurations, the current interpretations of structural changes differ from those of previous macroscopic-microscopic calculations [19]. The predicted transitional quadrupole moments were provided for future lifetime measurement to verify the current interpretations.

ACKNOWLEDGMENTS

The current work is supported by National Natural Science Foundation of China (Grant No. 11705038). I thank the HPC Studio at Physics Department of Harbin Institute of Technology for computing resources allocated through INSPUR-HPC@PHY.HIT.

[1] A. Bohr and B. R. Mottelson, *Nuclear Structure*, Vol. II (W. A. Benjamin, Reading, 1975).
[2] S.G. Nilsson and I. Ragnarsson, *Shapes and Shells in Nuclear Structure* (Cambridge University Press, Cambridge, 1995).
[3] R. Bengtsson, H. Frisk, F. May, and J. Pinston, Nucl. Phys. A **415**, 189 (1984).
[4] S. Frauendorf and J. Meng, Nucl. Phys. A **617**, 131 (1997).
[5] S. Frauendorf, Rev. Mod. Phys. **73**, 463 (2001).
[6] S. W. Ødegård, G. B. Hagemann, D. R. Jensen, M. Bergström, B. Herskind, G. Sletten, S. Törmänen, J. N. Wilson, P. O. Tjøm, I. Hamamoto, K. Spohr, H. Hübel, A. Görgen, G. Schönwasser, A. Bracco, S. Leoni, A. Maj, C. M. Petrache, P. Bednarczyk, and D. Curien, Phys. Rev. Lett. **86**, 5866 (2001).
[7] E. S. Paul, P. J. Twin, A. O. Evans, A. Pipidis, M. A. Riley, J. Simpson, D. E. Appelbe, D. B. Campbell, P. T. W. Choy, R. M. Clark, M. Cromaz, P. Fallon, A. Görgen, D. T. Joss, I. Y. Lee, A. O. Macchiavelli, P. J. Nolan, D. Ward, and I. Ragnarsson, Phys. Rev. Lett. **98**, 012501 (2007).
[8] J. Ollier, J. Simpson, X. Wang, M. A. Riley, A. Aguilar, C. Teal, E. S. Paul, P. J. Nolan, M. Petri, S. V. Rigby, J. Thomson, C. Unsworth, M. P. Carpenter, R. V. F. Janssens, F. G. Kondev, T. Lauritsen, S. Zhu, D. J. Hartley, I. G. Darby, and I. Ragnarsson, Phys. Rev. C **80**, 064322 (2009).
[9] M. Mustafa, J. Ollier, J. Simpson, M. A. Riley, E. S. Paul, X. Wang, A. Aguilar, M. P. Carpenter, I. G. Darby, D. J. Hartley, R. V. F. Janssens, F. G. Kondev, T. Lauritsen, P. J. Nolan, M. Petri, J. M. Rees, J. P. Revill, S. V. Rigby, C. Teal, J. Thomson, C. Unsworth, S. Zhu, B. G. Carlsson, H. L. Ma, T. Mufti, and I. Ragnarsson, Phys. Rev. C **84**, 054320 (2011).
[10] J. Ollier, J. Simpson, M. A. Riley, E. S. Paul, X. Wang, A. Aguilar, M. P. Carpenter, I. G. Darby, D. J. Hartley, R. V. F. Janssens, F. G. Kondev, T. Lauritsen, P. J. Nolan, M. Petri, J. M. Rees, S. V. Rigby, C. Teal, J. Thomson, C. Unsworth, S. Zhu, A. Kardan, and I. Ragnarsson, Phys. Rev. C **83**, 044309 (2011).
[11] A. Aguilar, D. B. Campbell, K. Chandler, A. Pipidis, M. A. Riley, C. Teal, J. Simpson, D. J. Hartley, F. G. Kondev, R. M. Clark, M. Cromaz, P. Fallon, I. Y. Lee, A. O. Macchiavelli, and I. Ragnarsson, Phys. Rev. C **77**, 021302 (2008).
[12] T. Bengtsson and I. Ragnarsson, Nucl. Phys. A **436**, 14 (1985).
[13] Y. Shi, J. Dobaczewski, S. Frauendorf, W. Nazarewicz, J. C. Pei, F. R. Xu, and N. Nikolov, Phys. Rev. Lett. **108**, 092501 (2012).
[14] Y. Shi, C. L. Zhang, J. Dobaczewski, and W. Nazarewicz, Phys. Rev. C **88**, 034311 (2013).
[15] A. V. Afanasjev, Y. Shi, and W. Nazarewicz, Phys. Rev. C **86**, 031304 (2012).
[16] C. M. Petrache, G. Lo Bianco, D. Ward, A. Galindo-Uribarri, P. Spolaore, D. Bazzacco, T. Kröll, S. Lunardi, R. Menegazzo, C. Rossi Alvarez, A. O. Macchiavelli, M. Cromaz, P. Fallon, G. J. Lane, W. Gast, R. M. Lieder, G. Falconi, A. V. Afanasjev, and I. Ragnarsson, Phys. Rev. C **61**, 011305 (1999).
[17] C. M. Petrache, S. Frauendorf, M. Matsuzaki, R. Leguillon, T. Zerrouki, S. Lunardi, D. Bazzacco, C. A. Ur, E. Farnea, C. Rossi Alvarez, R. Venturelli, and G. de Angelis, Phys. Rev. C **86**, 044321 (2012).
[18] C. M. Petrache, I. Ragnarsson, H.-L. Ma, R. Leguillon, T. Konstantinopoulos, T. Zerrouki, D. Bazzacco, and S. Lunardi, Phys. Rev. C **88**, 051303 (2013).
[19] C. M. Petrache, I. Ragnarsson, H.-L. Ma, R. Leguillon, T. Zerrouki, D. Bazzacco, and S. Lunardi, Phys. Rev. C **91**, 024302 (2015).
[20] M. Bender, P.-H. Heenen, and P.-G. Reinhard, Rev. Mod. Phys. **75**, 121 (2003).
[21] J. Dobaczewski, W. Satuła, B. Carlsson, J. Engel, P. Olbratowski, P. Powałowski, M. Sadziak, J. Sarich, N. Schunck, A. Staszczak, M. Stoitsov, M. Zalewski, and H. Zduńczuk, Comput. Phys. Commun. **180**, 2361 (2009).
[22] P. Olbratowski, J. Dobaczewski, J. Dudek, and W. Płóciennik, Phys. Rev. Lett. **93**, 052501 (2004).

[23] J. Bartel, P. Quentin, M. Brack, C. Guet, and H.-B. Håkansson, Nucl. Phys. A **386**, 79 (1982).
[24] E. Chabanat, P. Bonche, P. Haensel, J. Meyer, and R. Schaeffer, Nucl. Phys. A **635**, 231 (1998).
[25] J. Dobaczewski and J. Dudek, Phys. Rev. C **52**, 1827 (1995).
[26] M. Bender, J. Dobaczewski, J. Engel, and W. Nazarewicz, Phys. Rev. C **65**, 054322 (2002).
[27] J. Dobaczewski and J. Dudek, Comput. Phys. Commun. **102**, 183 (1997).
[28] P. Ring and P. Schuck, *The Nuclear Many-Body Problem* (Springer, Berlin, 1980).
[29] G. de Angelis, M. A. Cardona, M. De Poli, S. Lunardi, D. Bazzacco, F. Brandolini, D. Vretenar, G. Bonsignori, M. Savoia, R. Wyss, F. Terrasi, and V. Roca, Phys. Rev. C **49**, 2990 (1994).
[30] F. L. Bello Garrote, A. Görgen, C. Mihai, T. Abraham, L. C. Campo, J.-P. Delaroche, D. Filipescu, N. M. Florea, I. Gheorghe, D. G. Ghita, M. Girod, T. Glodariu, K. Hadyńska-Klęk, M. Klintefjord, J. Libert, R. Lica, T. Marchlewski, N. Marginean, R. Marginean, I. Mitu, A. Negret, C. R. Nita, F. Nowacki, A. Olacel, S. Pascu, T. Renstrøm, E. Sahin, S. Siem, J. Srebrny, A. Stolarz, L. Stroe, S. Toma, T. G. Tornyi, and A. Tucholski, Phys. Rev. C **97**, 064310 (2018).